Published in final edited form as:

J Immunol. 2020 April 01; 204(7): 1954–1967. doi:10.4049/jimmunol.1901134.

Macrophage migration and phagocytosis are controlled by Kindlin-3 link to cytoskeleton

Huan Liu[1,#], **Liang Zhu**[2,#], **Tejasvi Dudiki**[1], **Benjamin Gabanic**[1], **Logan Good**[1], **Eugene A. Podrez**[3], **Olga A Cherepanova**[2], **Jun Qin**[2,*], **Tatiana V. Byzova**[1,*]

[1]Department of Neurosciences, Lerner Research Institute, Cleveland Clinic, 9500 Euclid Ave, Cleveland, OH 44195

[2]Department of Cardiovascular & Metabolic Sciences, Lerner Research Institute, Cleveland Clinic, 9500 Euclid Ave, Cleveland, OH 44195

[3]Department of Inflammation and Immunity, Lerner Research Institute, Cleveland Clinic, 9500 Euclid Ave, Cleveland, OH 44195

Abstract

Major myeloid cell functions from adhesion to migration and phagocytosis are mediated by integrin adhesion complexes, also known as adhesome. The presence of a direct integrin binding partner Kindlin-3 is crucial for these functions and its lack causes severe immunodeficiency in humans. However, how Kindlin-3 is incorporated into the adhesome, and how its function is regulated, is poorly understood. Here, using NMR we show that Kindlin-3 directly interacts with PXN (Paxillin) and LPXN (Leupaxin) via G43/L47 within its F0 domain. Surprisingly, disruption of Kindlin-3-PXN/LPXN interactions in Raw 264.7 macrophages promoted cell spreading and polarization, resulting in upregulation of both, general cell motility and directed cell migration, which is in a drastic contrast to the consequences of Kindlin-3 knockout. Moreover, disruption of Kindlin-3-PXN/LPXN binding promoted the transition from mesenchymal to amoeboid mode of movement as well as augmented phagocytosis. Thus, these novel links between Kindlin-3 and key adhesome members, PXN/LPXN limit myeloid cell motility and phagocytosis, thereby providing an important immune regulatory mechanism.

Keywords

Adhesion; Kindlin-3; PXN; LPXN; migration; blebbing; phagocytosis

[*]To whom correspondence should be addressed: Tatiana V. Byzova (Phone number: 216-445-4312; byzovat@ccf.org); Jun Qin (Phone number: 216-444-5392; qinj@ccf.org).

[#]These authors contributed equally to this work.

Author Contributions: H.L, L.Z, J.Q and T.V.B conceived this study. H.L designed and performed experiments, analyzed data, wrote and edited the original draft. H.L, B.G, T.D and L.G performed all of the cell biology experiments, L.Z purified proteins and performed NMR 2D-HSQC and HSQC titration, and also wrote and edited the manuscript. T.V.B, J.Q, H.L, L.Z, E.P, O.C, and B.G reviewed and revised the manuscript. J.Q and T.V.B conceived experiments, interpreted the data and wrote the manuscript. T.V.B secured funding.

Conflict of interest: The authors declare that they have no conflicts of interest with the contents of this article.

Introduction

Cells of myeloid origin including macrophages, function in immune surveillance and defense. These functions are critical for a wide range of physiological and pathological processes, ranging from development, metabolism, tissue homeostasis, injury response, and regeneration, to human pathologies from cancer to neurodegenerative disorders (1). Their function is dependent on the timely recruitment from blood stream, a process involving adhesion to endothelium and subsequent transmigration; followed by directed migration to the site of inflammation and engulfment (phagocytosis) of substances ranging from bacteria to necrotic cells (2–4). Irregularities in the execution of these defensive functions, including either insufficient or excessive performance, result in serious pathological complications arising from immune incompetence to diseases associated with chronic inflammation. All of the processes described above are mediated by integrins, which are cell-surface receptors for the extracellular matrix. While extracellular domains of integrins bind to their respective ligands either on the surface of bacteria or apoptotic cells or within an extracellular matrix, their cytoplasmic domains interact with a regulatory “adhesome” network of >200 molecules (5, 6). Among these, two direct binding partners of integrins, Talin and Kindlin are absolutely required for their function (7). In myeloid cells of both resident (e.g. microglia), and non-resident, i.e. recruited from blood, origin, Kindlin-3 represents the main Kindlin paralog, and a lack of Kindlin-3 in humans leads to severe immunodeficiency, bone problems, and bleeding (8). Kindlin-3-null cells are not recruited to sites of inflammation due to deficiencies in integrin activation-dependent firm adhesion to endothelium, which, together with a number of other defects in integrins result in immune incompetence (8, 9). The defects in Kindlin-3 null cells are expected to prohibit cell migration, which is true for 2-dimensional (2D) experiments and *in vivo* processes that are dependent on integrin activation, such as monocyte recruitment (10). However, myeloid cells exhibit two interchangeable migration modes, namely mesenchymal and amoeboid migration (3, 4). While the mesenchymal migration is dependent on integrins and actin polymerization driven-sheet-like lamellipodia, integrin-independent amoeboid migration relies upon tissue pressure- dependent-spherical blebs or actin-rich finger-like filopodia and is considered to be faster (11–14). The lack of adhesion, increase in cortical contractility as well as cell confinement promote the formation of cell “blebs” and mesenchymal to amoeboid transition (MAT) (15–18). Indeed, neither the lack of integrins, Talin (19) nor Kindlin-3 (10) interferes with amoeboid migration in vivo. At the same time, the mechanisms underlying the transition between these two important migration modes are poorly understood.

All Kindlins directly bind to membrane phosphatidylinositol-(4, 5)-bisphosphate (PIP2) via their pleckstrin homology (PH) domain (20, 21) and to the cytoplasmic domain of the beta-subunit of integrins via their F3 domain (QW615) (10, 20, 22). Kindlin-2 was also shown to interact with integrin-linker-kinase (ILK) via its F2PH domain (23), as well as with F-actin (24) and cytoskeleton protein PXN (25, 26) via its F0 domain (27). Importantly, these Kindlin-2 interactions promote integrin-dependent functions, e.g. cell spreading (23, 26, 28). For instance, Kindlin-2-PXN interactions positively regulate fibroblast adhesion, spreading, the formation of focal adhesions, and cell migration (25–27, 29). The same applies to the interactions between Kindlin-2 and ILK (23) as well as Kindlin-2 and actin (24). To date, no

interactions negatively regulating or restricting integrin functions are known for Kindlins. In addition, despite the importance of Kindlin-3 in myeloid and other hematopoietic cells, its exact role, as well as the mechanisms and consequences of its interactions with adhesome components, are poorly understood. Since these findings have mainly been based on domain-deletion or knockout studies, which affect interactions with dozens of binding partners, they generate significant controversies (25, 26, 29). Accordingly, we have based our studies on the structural analysis of the binding interfaces between Kindlin-3 and PXN, and its homolog LPXN through the generation of point mutations and detailed analysis of integrin-mediated functions in myeloid cells. We show that in contrast to other known Kindlins binding partners, interactions between Kindlin-3 and PXN/LPXN negatively regulate integrin-dependent functions of myeloid cells. While Kindlin-3 knockout prevents integrin-mediated responses, and Kindlin-3 binding to integrin cytoplasmic domain does not affect the Kindlin-3-PXN/LPXN interaction, disruption of Kindlin-3-PXN/LPXN affects integrin β1 activation. Kindlin-3 mutant lacking interactions with PXN/LPXN show enhanced cell spreading, membrane blebbing, migration as well as macrophages phagocytosis. Moreover, the consequences of these interactions on integrin-mediated responses are opposite for Kindlin-3 and Kindlin-2, despite the conserved nature of the interaction site.

Materials and Methods

Plasmid constructs

Human Kindlin-3 Open Reading Frame (ORF) from pGFP-hKindlin3 (8) was sub-cloned into plvx-Dsred-monomer-c1 (Clontech) and PCMV-HA-N (Clontech) vectors. PGFP-hKindlin3 was changed from GFP to Flag tag. Human PXN (paxillin-γ) ORF and human LPXN ORF (OriGene Technologies) were subcloned into Pmcv-N-myc vector (Clontech). The following constructs were used for protein expression in the bacterial system: human Kindlin-3 F0 (1–105), human PXN (paxillin-γ) LIM4 (541–605) and human LPXN LIM4 (324–386) subcloned into pGST-1 (glutathione S-transferase) vectors. Kindlin-3 F0 double mutant (G43K, L47E) and Kindlin-3 integrin binding site mutant (K3KI) were generated by using a QuickChange lightning site-directed mutagenesis Kit (Agilent Technologies) and Kindlin-3 F0 deletion (lack of 1–106) was generated by PCR.

Cell culture

Raw 264.7 cells, NIH3T3 cells, HEK 293 cells, and 293T phoenix cells were cultured in DMEM medium (Gibco) supplemented with 10% Fetal Bovine Serum (FBS) (Gibco) and 50 μg/ml Penicillin/ Streptomycin (Gibco). Thp1 cells, K562 cells, Jurkat cells, MPM cells, and L929 cells were cultured in RPMI1640 medium (Gibco) supplemented with 10% FBS (Gibco) and 50 μg/ml Penicillin/ Streptomycin (Gibco). SIM-A9 cells were cultured in DMEM: F12 medium (Gibco) supplemented with 5% FBS (Gibco), 5% horse serum (Gibco) and 50 μg/ml Penicillin/ Streptomycin (Gibco). BMDM were cultured in RPMI1640 medium (Gibco) supplemented with 10% FBS (Gibco), 50 μg/ml Penicillin/ Streptomycin (Gibco) and 30% L929 conditional medium.

Protein expression and purification

GST-tagged protein (Kindlin-3 F0, PXN LIM4 or LPXN LIM4) was expressed in *E.coli* BL21 (DE3) strain (New England Biolabs). Bacteria were initially grown in 50 mL Lysogeny broth (LB) medium and then amplified in 1~2 L LB at 37 °C. The culture was induced by 0.4 mM isopropyl β-D-1-thiogalactopyranoside (IPTG) at room temperature (RT) overnight when it reached an A_{600} of 0.7. The pellet was collected and suspended in buffer, and then frozen at −80 °C. For protein purification, the pellet was lysed and the lysate was subjected to high-speed centrifugation. The supernatant was collected and incubated with glutathione-Sepharose 4B resin (GST beads) at 4 °C for 2 hours. GST-tagged protein was eluted by buffer containing 50 mM Tris-HCl (pH 8.0), 150 mM NaCl and 10 mM Glutathione (GSH). By performing the buffer exchange, the GST-tagged protein was finally stored in buffer which contained 50 mM Tris-HCl, pH 8.0, 150 mM NaCl and 0.5 mM tris (2-carboxyethyl) phosphine (TCEP). For the protein used in Nuclear Magnetic Resonance spectroscopy (NMR) experiments, the GST tag was removed by TEV protease. After incubation with GST beads, the untagged protein was collected and subjected to gel filtration by using Superdex-75 (16/60) (GE Healthcare) which was pre-equilibrated with the buffer containing 50 mM NaH_2PO_4/Na_2HPO_4 (pH 6.8), 50 mM NaCl, and 0.5 mM TCEP. ^{15}N-labeled proteins used in NMR studies were achieved by growing bacteria in minimal medium (MM) with $^{15}NH_4Cl$ as the sole nitrogen source. For expression of the ^{15}N -labeled PXN LIM4 or LPXN LIM4 domain, $ZnCl_2$ was added into the MM to reach a concentration of 50 μM during IPTG induction. Protein concentration was measured by absorbance at 280 nm.

GST pull-down

HEK293 cells were transfected with indicated plasmids by Lipofectamine 3000 (Thermo Fisher). 48-hours post-transfection, cells were lysed with lysis buffer (10 mM Tris PH 7.5, 100mM NaCl, 1%Nonidet P-40, 50 mM NaF, 1.5 mM Na_3VO4, protease inhibitor mixture (Roche), 1 mM DTT, and 1 mM PMSF) and then incubated with 10 μg of recombinant GST or GST-fusion proteins which was pre-immobilized to 20 μL of Glutathione Agarose (Pierce) at 4ºC for 2 hours. GST-agaroses were then washed 4 times with the washing buffer (10 mM Tris PH 7.5, 300mM NaCl, 1%Nonidet P-40, and 50 mM NaF) and boiled in SDS sample buffer before analysis by western blotting.

Western blotting

Western blotting was performed using a standard protocol. Briefly, cells were lysed with 1% SDS lysis buffer and protein concentrations were determined using the BCA Assay Kit (Thermo Fisher Scientific). Protein samples were resolved on 10% SDS-PAGE (Bio-rad) and then transferred to PVDF membranes (Millipore). Membranes were blocked with 5% non-fat milk and then incubated sequentially with primary and secondary antibodies. After washing with 1×TBST buffer, the membrane was detected by ECL Detection Reagent (Thermo Fisher Scientific). The following antibodies were used for western blotting: GAPDH (D16H11) Rabbit mAb (Catalog# 5174, Cell Signaling Technology), Myc-Tag (9B11) Mouse mAb (Catalog#2276S, Cell Signaling Technology), HA-Tag (C29F4) Rabbit antibody (Catalog#3724S, Cell Signaling Technology), Flag M2 antibody ANTI-FLAG

produced in rabbit (Catalog# F7425, Sigma), GST Tag Antibody (8–326) (Catalog# MA4–004, Thermo Fisher Scientific), Rabbit-anti-human-paxillin (H-114) (Catalog# sc-5574, Santa Cruz), Rabbit Kindlin-3 Antibody (Catalog# ab68040, Abcam), Mouse Anti-Kindlin-2 (clone 3A3)(Catalog# MAB2617, Millipore), and Mouse Anti-Hic5 (Clone 34) antibody (Catalog#611164, BD biosciences). The secondary antibodies for western blotting were purchased from Cell Signaling Technology.

RNA isolation and qRT (quantitative real-time) PCR

Total RNA was isolated from cells using Trizol reagent (Thermo Fisher Scientific) according to the manufacturer's instructions. cDNA was synthesized by reverse transcription using PrimeScrip RT Master Mix (Takara) and subjected to RT- PCR with SYBR Green (Bio-rad) and gene-specific primers. Relative mRNA levels were calculated by normalization to hypoxanthine phosphoribosyltransferase 1 (HPRT) mRNA using the ΔΔCt method.

NMR 2D-HSQC and HSQC titration

2D-HSQC (**heteronuclear single quantum coherence**) experiments were performed on a Bruker 600 MHz NMR spectrometer. Samples containing 100 μM ^{15}N-labeled PXN LIM4 or LPXN LIM4 in the absence or presence of Kindlin-3 F0 were studied. Experiments were performed at 25 °C in buffer containing 50 mM NaH_2PO_4/Na_2HPO_4 (pH 6.8), 50 mM NaCl, 0.5 mM tris (2-carboxyethyl) phosphine (TCEP) and 5% D_2O. For HSQC titration, 100 μM ^{15}N-labeled LIM4 PXN LIM4 or LPXN LIM4 was mixed with increasing concentrations of Kindlin-3 F0 to collect 2D-HSQC spectra. The chemical shift changes of six independent, well-resolved residues were fit to obtain the dissociation constant (K_d) by using an online analysis tool (http://supramolecular.org/) (30). Chemical shift change ($\Delta\delta_{obs\ [HN,\ N]}$) of each residue was calculated with the equation $\Delta\delta_{obs\ [HN,N]} = [(\Delta\delta_{HN}W_{HN})^2 + (\Delta\delta_N W_N)^2)]^{1/2}$ where $\Delta\delta$ (ppm) = $\delta_{bound} - \delta_{free,}$ and W_{HN} and W_N are weighting factors (W_{HN} = 1, W_N = 0.154).

Flow cytometry analysis

For cell sorting of the similar level of Ds-red positive cells, cells were suspended into sorting buffer which contained 25mM HEPES (pH 7.0), 1x Phosphate Buffered Saline (Ca^{2+}/Mg^{2+} free), 1mM EDTA, and 1% Fetal Bovine Serum (Heat-Inactivated), and then sorted through a BD flow cytometer using the same gate.

For Ds-red signal detection, cells were suspended into 5%FBS/ phosphate-buffered saline (PBS). Data were then collected in a BD flow cytometer and analyzed by Flow Jo software.

For apoptosis analysis, the indicated Raw 264.7 cells were cultured in the tissue culture plates for 24 hours and Control cells were treated with 10 μM Camptothecin (Sigma) at 37 °C for 1 hour to induce apoptosis as the positive control. Then cells were harvested and stained with the FITC Annexin V Apoptosis Detection Kit I (BD biosciences). The data was collected by a BD flow cytometry and analyzed with Flow Jo software.

To detect C5a receptor surface expression, integrin expression and activation, the indicated Raw 264.7 cells were cultured in the tissue culture plates for 24 hours. Cells were then

harvested and stained with APC anti-mouse CD88 (C5aR) Antibody (Catalog#135807, Biolegend), APC Rat IgG2b, κ Isotype Ctrl Antibody (Catalog#400611, Biolegend), Alexa Fluor® 647 Rat Anti-CD11b (αM)(Catalog#557688, BD) and FITC-CD18 (Catalog#4336690, eBioscience) respectively at 4 °C for 30min, then washed and analyzed by flow cytometry. For integrin β1, Cells were harvest and stained with primary antibodies Rat-anti-mouse CD29 (9EG7) (Catalog#553157, BD) and Hamster Anti-Rat CD29 (Catalog#553837, BD) at 4 °C for 1 h, then fixed with 2% PFA at RT for 15min, washed and stained with secondary antibodies Alexa-Fluor 488-goat anti-rat (Catalog# A11006, Thermo Fisher Scientific) and Alexa-Fluro 647-Affinipure goat anti-Syrian Hamster IgG (H+L) (Catalog#107–606-142, Jackson lab) at 4°C for 30min, then washed. Data was collected by BD flow cytometry and analyzed with Flow Jo software.

Fibrin gel preparation

K3KO-expressed Ds-red-hK3 Raw 264.7 cells were labeled with PKH67 (Sigma-Aldrich) and Ds-red-hK3-GKLE cells were labeled with PKH26 (Sigma-Aldrich) according to the manufacturer's instructions, and then mixed at a 1:1 ratio. Fibrin gel was made by labeled cells, 2 mg/mL fibrinogen (Sigma-Aldrich), 1% FBS, 1% penicillin/streptomycin, and 0.5 U/mL thrombin (Sigma-Aldrich) and formed at 37 °C for 1 hour, then analyzed using a Leica confocal microscope.

Immunofluorescence imaging

For cell spreading and cell protrusions analysis, Raw 264.7 cells were seeded on fibronectin and 0.1% PLL (Poly-L-Lysine Solution, Santa Cruz, sc-286689) pre-coated coverslips for 1 hour, and treated with or without 20 ng/ml anaphylatoxin complement 5a (C5a) (R & D Systems and 2150-C5–025) for 2 hours. Then cells were washed with cold PBS, fixed with 4% paraformaldehyde for 15 min, permeabilized with 0.1%Triton X-100 for 5min, blocked in 3% BSA/10% goat serum/PBS for 30 min, and incubated with anti-PXN antibody (Catalog# sc-5574, Santa Cruz), and Alexa Fluor™ 647 Phalloidin (Catalog# A22287, Thermo Fisher Scientific) in blocking buffer overnight at 4 ºC. After washing with PBS, cells were incubated with Goat anti-Rabbit IgG (H+L) Cross-Adsorbed Secondary Antibody Alexa Fluor 488 (Catalog# A-11008, Thermo Fisher Scientific) for 1.5 hours, then washed and mounted with ProLong® Gold Antifade Mountant with DAPI (Thermo Fisher Scientific). Images were collected using a Leica confocal microscope and quantified by Image J software. Both smaller and bigger protrusions were counted in all the cells.

For cell blebs analysis, Raw 264.7 cells were labeled with PKH67 (Sigma-Aldrich) according to the manufacturer's instructions, and seeded on the coverslip for 20min, then washed with cold PBS, fixed, and proceeded general immunofluorescence staining and pictured by Leica confocal microscope.

Time-lapse live imaging

For cell blebs, cells in media (2D) or in fibrin gels (3D) were seeded onto 3.5μm glass-bottom dishes (Mat Tek, catalog# P35G-1.5–14-C) and recorded by DIC (Differential interference contrast) and z-stack with a 40× dry objective using the Leica TCS-SP8-AOBS inverted confocal microscope (Leica microsystems, GmbH, Germany) configured with HC-

PL FLUOTARL 40×/0.75 Dry object and OKO Touch Stage top incubator (Okolab USA Inc, San Bruno, CA). Image analysis was performed using LAS X (Leica application suite X) software. The protrusions ratio and the relative lifetime of protrusions were quantified from frame to frame of the videos.

For cell migration, cells were cultured in fibronectin pre-coated 12-well-plates (Corning). Time-lapse recordings were acquired with Leica DMI6000 inverted microscope and LASX software (Leica microsystems, GmbH, Wetzlar Germany) equipped with HC-PL FLUOTARL 20×/0.4 Dry object, a Hamamatsu Image EM CCD camera and a Hamamatsu Flash4 camera (Hamamatsu Photonics, Shizuoka, Japan), PECON Large Chamber incubator, heating unit 2000, CO2 controller, and temp control 37–2 Digital 2-Channel (PECON GMBH, Germany) every 5 min for 24 hours, then images were transformed into videos by LAS X (Leica application suite X) software, extracted every 5 pictures with 25min-interval and quantified by image pro plus software. All the cells were counted without distinguishing the morphology. Cell trajectories were drawn by Chemotaxis and Migration software.

Transwell-cell migration assay

Raw 264.7 cells were serum-starved for 12 h. Cells (1×10^5) were seeded into the 6.5 μm-pore size inserts and induced by serum and 20ng/ml C5a for 24 hours. Cells were then fixed and stained with 0.5% crystal violet. The bottom sides of the inserts were imaged and quantified by Image J software.

Phagocytosis assay

Latex beads (Catalog# L4530, Sigma-Aldrich) were opsonized with C3bi by incubating with Human IgM (Sigma-Aldrich) and fresh mouse serum at 37°C for 1 hour. Raw 264.7 cells were incubated with C3bi-opsonized Latex beads with or without 150nM Phorbol myristate acetate (PMA) at 37°C for 2 hours, then fixed, permeabilized, stained with anti-RFP antibody (Catalog#ab62341, Abcam) and imaged by confocal microscopy using z-stack. The number of beads phagocytized by Raw 264.7 cells was quantified by Image J software.

CRISPR-Cas9 mediated knockout

CRISPR-Cas9 technology was used to generate Kindlin-3 knockout cells. Two independent sgRNAs were designed by the Zhang laboratory CRISPR Design Tool. Annealed oligonucleotides were ligated into the vector LentiCRISPRv2 (Addgene, Feng Zhang's lab) and digested with BsmBI (Fermentas). Lentiviral infection was performed with Lenti-X™ Packaging Single Shots (Clontech) in accordance with a Cleveland Clinic IBC protocol. After 72 hours, cells were selected with 2 μg/mL puromycin (Thermo Fisher Scientific) for another 48 hours. Live cells were collected and sorted by flow cytometry into 96-well plates. Individual clones were examined by western blotting or genomic DNA sequencing. The sgRNA primers sequence for K3KO are as follows:

K3KO#1, forward:	*CACCGACGGGGGAGTCGCACATTGG*
K3KO#1, reverse:	*AAACCCAATGTGCGACTCCCCCGTC.*

K3KO#2, forward:	*CACCGACAGACGTGTGCTGCGGCTT*
K3KO#2, reverse:	*AAACAAGCCGCAGC ACACGTCTGTC*

Overexpression of hKindlin-3 by lentiviral infection

The lentivirus infection was performed in accordance with the Cleveland Clinic IBC protocol. For overexpression, Phoenix packaging cells (Commercial) were transfected with plvx-Dsred-monomer-c1, plvx-Dsred-monomer-Kindlin-3 and plvx-Dsred-monomer-Kindlin-3-G43K/L47E by lipofectamine3000 (Thermo Fisher Scientific) for 48 hours. Then Raw 264.7 cells were infected by lentivirus from the culture medium with Lenti-X™ Packaging Single Shots (Clontech) according to commercial instructions. 72 hours later, cells were subjected to cell sorting for Ds-red positive cells (BD FACS Aria II, Cleveland Clinic), followed by western blotting and functional experiments.

Statistical analysis

Data are expressed as mean ± SEM. Differences were analyzed using Student's *t*-tests. Values less than 0.05 were considered significant. *p<0.05, **p<0.005, and ***p<0.001.

Results

Kindlin-3 interacts with-PXN/LPXN in a similar manner as Kindlin-2

The Kindlin family includes Kindlin-1, Kindlin-2 and Kindlin-3, which contain a conserved F0 domain at the N-terminal, an F1-F2 domain, a conserved PH domain, and an F2-F3 domain (Fig. S1A) (31, 32). Kindlin-3 is the only Kindlin that is expressed in myeloid cells including Raw 264.7 macrophage cells (Fig. S1B). The PXN family includes PXN, Hic5, and LPXN, with an LD-protein-protein interaction motif at the N-terminus and four LIM domains at the C-terminus (Fig. S1A) (33–35). Two members of the PXN family are present in Raw 264.7 cells: PXN and LPXN (Fig. S1B, S1C). 2D NMR HSQC revealed that the interaction between Kindlin-2 and PXN is mediated by the Kindlin-2 F0 domain and the PXN LIM4 domain (27). Disruption of Kindlin-2/PXN interaction by the key amino acids G42/L46 in F0 domain or F577/L579/K580 mutations in LIM4 domain severely impair focal adhesion formation and directed cell migration (27). Since G43/L47 are conserved in both Kindlin-2 and Kindlin-3 (Fig. S1D), we tested whether Kindlin-3 binds to PXN/LPXN in a similar fashion. First, Both GST-pull down and 2D-NMR HSQC confirmed the Kindlin-3-F0 domain interaction with both PXN-LIM4 and LPXN-LIM4 (Fig. 1A–1C). Interestingly, based on HSQC titration, the binding affinity of Kindlin-3 to PXN-LIM4 domain is nearly two times stronger than that of Kindlin-3 to LPXN-LIM4 (Fig. 1D, 1E), which is consistent with the results of the GST pull-down assay (Fig. 1C). Further, Kindlin-3-F0 deletion disrupted Kindlin-3-PXN interaction, suggesting only the F0 domain, but no other domains mediates Kindlin-3-PXN interaction (Fig. S1E). To specifically disrupt this interaction, we mutated the conserved interface residues G43 and L47 of Kindlin-3 (corresponding to G42 and L46 of Kindlin-2) (Fig. S1D) into Lysine and Glutamine respectively. Both GST-pull down and 2D-NMR HSQC showed that Kindlin-3-F0-G43K/L47E mutations are able to disrupt its binding to both PXN and LPXN LIM4 domains (Fig. 1F–1H, and S1F). Similar to

Kindlin-2, GST-pull down shows that F577/L579/K580 mutations in PXN-LIM4 domain also disrupted Kindlin-3-PXN interaction (Fig. S1E).Since NMR is used to assess weak protein-protein interactions (36), we were unable to verify by full-length Co-Immunoprecipitation. Instead, GST-pull down showed that full-length Flag-Kindlin-3, but not Flag-Kindlin-3-F0-G43K/L47E mutations, binds to PXN and LPXN LIM4 domain (Fig. 1I). Together, these results show that Kindlin-3-interact with PXN/LPXN interaction via the F0 and LIM4 domains, as well as the conserved residues within the F0 domain. Interestingly, disruption the integrin binding site (Kindlin-3 mutant, K3KI)(10) did not affect Kindlin-3-PXN/LPXN interaction (Fig. 1J, 1K), suggesting that Kindlin-3-PXN/LPXN interactions are integrin-independent.

Disruption of Kindlin-3-PXN/LPXN interaction promotes cell spreading, polarization and inhibits integrin activation

In order to understand the role of Kindlin-3-PXN/LPXN interactions in myeloid cells, we generated two independent clones of CRISPR-cas9-based Kindlin-3 knockout in Raw 264.7 cells, K3KO#1 and K3KO#2 (Fig. 2A, S2A, S2B), and then re-expressed human Kindlin-3 (hK3) and Kindlin-3-G43K/L47E (hK3pxn) mutant in these clones independently by lentiviral infection (A schematic is presented in Fig. 2A). Equal levels of protein re-expression were confirmed by flow cytometry (note that in all experiments, Kindlin-3 was re-expressed as a DS-Red fusion protein) (Fig. 2B) and further verified by western blotting (Fig. 2C). As expected, knockout of Kindlin-3 (K3KO) completely prevented cell adhesion, subsequent spreading, cell polarity and cell protrusions both in the presence and absence of an agonist C5a (Fig. 2D–2G). Re-expression of Kindlin-3 (hK3) in K3KO cells restored cell spreading and actin reorganization as shown by Phalloidin staining (Fig. 2H–2M). In comparison to hK3, expression of hK3pxn mutant augmented cell spreading (Fig. 2H, 2J). The area of hK3pxn expressing cells was ~30% higher (Fig. 2J) and the cell polarity index was >65% higher compared to hK3 expressing cells (Fig. 2I). Upon stimulation with C5a the situation was similar and hK3pxn cells exhibited augmented spreading compared to hK3 cells (Fig. 2J). Activation with C5a resulted in increased cell polarity by >2 fold in hK3 and >1.5 fold in hK3pxn, and the difference between these cell types was no longer apparent (Fig. 2K). Importantly, the number of cellular protrusions in hK3pxn mutant cells was >4 fold higher than in hK3 cells even in the absence of cell stimulation with agonist (Fig. 2I, quantification shown in Fig. 2L). Moreover, while C5a treatment promoted protrusions in hK3, their numbers did not reach the level observed upon expression of hK3pxn mutant, which was >85% higher compared to hK3 expressing cells (Fig. 2I, 2L). While there was no difference in the length of protrusions in native conditions, the length of protrusions increased after C5a treatment in hK3pxn mutant cells compared with hK3 cells (Fig. 2M).

Therefore, in contrast to Kindlin-2, disconnecting Kindlin-3 from PXN/LPXN promoted cell polarization, spreading and formation of actin-rich protrusions, in a similar manner to C5a agonist stimulation.

At the same time, flow cytometry revealed no difference in C5a Receptor (C5aR) surface expression between hK3 cells and hK3pxn cells (Fig. S2C-S2D), suggesting that the increase in cell spreading, cell polarity and cell protrusions in hK3pxn cells is not due to

altered expression level of C5aR. None of the used cell lines adhered to 0.1% PLL (Fig. S2E-S2H), thereby demonstrating that these effects are integrin-dependent. Expression of αMβ2 (CD11b/CD18) complex and β1 integrins was generally similar between hK3 and hK3pxn cells (Fig. S3A-S3D). Integrin β1 activation status measured by 9EG7 staining but not its expression was slightly decreased on hK3pxn cells compared to hK3 line, while similar to previous reports, no effect of C5a stimulation on β1 integrin status was observed (37).

Disruption of Kindlin-3-PXN/LPXN interactions promotes cell migration and transition from mesenchymal to amoeboid migration

Kindlins interact with the cell membrane via their PH domain and with the cytoskeleton, F-actin and PXN/LPXN via F0 domain, thereby linking the cell membrane with the cytoskeleton (21, 24–27, 29). Disruptions of similar intracellular links lead to increased and imbalanced cortical contractility, which, in turn, promote cell blebbing and facilitate the transition to the amoeboid mode of migration (17, 38). Thus, Kindlin-3-PXN/LPXN interactions might serve as the main connection to the cytoskeleton and its disruption might lead to increased blebbing and transition to amoeboid migration. Several models were used for this analysis: time-lapse-live imaging of spontaneous migration on the adhesive substrate in 2D, analysis of blebbing during cell spreading by immunofluorescent staining, evaluation of blebbing and lamellipodia formation during initial and late phases of cell spreading by time-lapse-live imaging, apoptosis analysis by flow cytometry, directed cell migration toward substrate, and finally, blebs and lamellipodia analysis by time-lapse-live imaging under confinement conditions in 3D, known to promote blebbing and trigger amoeboid mode.

Kindlin-3 deficiency prevented spontaneous cell movement on the adhesive substrate in 2D as evidenced by time-lapse live-imaging (Fig. 3A, 3B and Videos 1–2). The average cell velocity was reduced by two-fold in K3KO cells (Fig. 3B), and K3KO cells were not moving along the substrate, but merely exhibited the movements of the membrane (cell migration trajectories in Fig. 3A and Video 2).

In the absence of Kindlin-3 cells formed more actin-deficient blebs compared to control cells (Fig. 3C, 3D). Differential Interference Contrast (DIC) microscopy revealed that K3KO cells had more spherical blebs during initial stages of cell adhesion as compared to control cells, which remained relatively smooth (Fig. 3E, 3F and Videos 3–4). Quantification of membrane movements revealed that while control cells primarily formed lamellipodia, both K3KO1 and K3KO2 lines exhibited extensive blebbing (Fig. 3F). In most cases, the phenotype of K3KO#2 cells was more apparent due to the specifics of K3 excision (Fig.S2A). The protrusions turned over quickly with a similar lifetime in control and K3KO cells (Fig. S4A). At later stages, when cells firmly adhered to the substrate (14–18 hours after seeding), control cells formed lamellipodia primarily in one direction, whereas K3KO cells continued producing numerous spherical blebs covering the nearly entire surface of the cell (Fig. 3G, 3H and Videos 5–6). Thus, while the lack of Kindlin-3 significantly impairs cell velocity on the substrate and directed migration (10), it induces the attributes of amoeboid migration mode, namely the switch from the directional lamellipodia to excessive

membrane blebbing (16). While control cells primarily formed lamellipodia and filolopodia, K3KO cells exhibited blebbing (Fig. 3G, 3H). The protrusions in K3KO cells had substantially shorter lifetime than in control cells, while exhibiting no lamellipodia (Fig. 3I). The relative lifetime of filopodia decreased by >5 fold in K3KO compared to control cells (Fig. 3I). To verify that increased blebbing is not due to apoptosis, we stained these cells for Annexin V (Fig.S3I, S3J). The rate of spontaneous apoptosis in K3KO lines was not higher compared to control cells. Moreover, re-expression of hK3 in K3KO cells did not affect apoptosis rate demonstrating that increased blebbing in K3KO cells is not due to apoptosis (Fig.S3I, S3J). Together, the lack of Kindlin-3 diminishes cell adhesiveness, while increasing cell blebbing and promoting membrane protrusions turnover, which, together are likely to aid fast amoeboid migration.

Re-expression of hK3 in K3KO cells reverted the membrane movement and migration velocity on the substrate (Fig. 4A and Videos 7, 9 and 11). In fact, the behavior of cells re-expressed hK3 (Videos 9 and 11) was indistinguishable from that of control cells (Videos 3 and 5). Cells expressing hK3pxn mutant exhibited a unique set of characteristics, namely, substantial spreading on the substrate similar to or greater than that of hK3 cells and at the same time, a high level of membrane blebbing resembling K3KO cells (Videos 10 and 12). Importantly, the average velocity on the substrate of hK3pxn mutant-expressing cells was ~1.5 fold higher compared to hK3 cells (Fig. 4A, 4B). Immunofluorescent staining showed that the number of actin-deficient membrane blebs increased in hK3pxn cells compared to hK3 cells by ~3.5 fold on K3KO#1 background and by ~9 fold on K3KO#2 background (Fig. 4C, 4D). DIC microscopy time-lapse imaging showed that while hK3 cells formed primarily lamellipodia (more than 50% of the cells), the proportion of lamellipodia was substantially lower (less than 30%) in hK3pxn mutant cells, and cell blebbing in hK3pxn mutant cells was respectively higher compared to hK3 cells (Fig. 4E, 4F and Video 9–10). Similarly, the protrusions in both hK3 cells and hK3pxn cells turned over quickly with a similar lifetime during initial spreading stage (Fig. S4B). Consistently, during the firm adhesion stage when membrane blebbing has generally ceased and transitioned to lamellipodia/filopodia in hK3 cells, hK3pxn mutant cells continued with intense blebbing (~37% blebs in K3KO#1 and ~20% in K3KO#2) as compared to hK3 expressing cells at ~4 and 15%, respectively (Fig. 4G–4H and Videos 11–12). Moreover, certain hK3pxn mutant cells transitioned from filopodia formation to blebbing (Fig. 4G, 4H and Video 12). The protrusions in hK3pxn cells turned over much faster than in hK3 cells (Fig. 4I). The relative lifetime of lamellipodia decreased by ~ 20% and by ~4.5 fold in hK3pxn mutant cells compared with hK3 on the background of K3KO#1and K3KO#2, respectively (Fig. 4I). The relative lifetime of filopodia in hK3pxn vs hK3 cells decreased by 1.4 and 2 fold in K3KO#1 and K3KO#2 lines, respectively, (Fig. 4I). Apoptosis analysis by Annexin V staining revealed no significant difference between hK3 and hK3pxn cells (Fig. S3I, S3J), demonstrating that high membrane blebbing in hK3pxn cells is not due to apoptosis. Together, these results show that disruption of Kindlin3-PXN/LPXN interactions augmented cell blebbing and protrusions turnover, indicating the shift towards amoeboid mode.

Next, directed cell migration toward anaphylatoxin complement 5a (C5a), which is a ligand and agonist for myeloid cells (39–41), was assessed in Boyden chambers. As shown previously, Kindlin-3 knockout nearly completely abolished directed cell migration, whereas

re-expression of hK3 completely restored this response (Fig. 5A, 5B). This is consistent with the concept that expression of Kindlin-3 is critical for the function of integrins (8, 10). A direct comparison between migrating hK3 and hK3pxn cells is shown in Fig. 5A and the quantification is in Fig. 5B. The number of hK3pxn mutant cells transmigrated toward C5a was ~37% higher compared to hK3 cells (Fig. 5B), demonstrating that Kindlin3-PXN/LPXN interactions limit directed macrophage migration.

Since amoeboid migration is generally restricted to 3D conditions, it is expected that the blebbing phenotype of mutant cells will be augmented in 3D, where pressure from the substrate promotes amoeboid behavior (12, 42). Cells expressing hK3 and hK3pxn mutant were labeled with green and red dyes PKH67 and PKH26, respectively, and were imaged next to each other at different depths within a fibrin gel (Fig. 5C, 5D and Video 13) without interference from the fluorescence of the fusion protein (Fig. S4C, S4D). This analysis revealed a substantially higher frequency of blebbing in hK3pxn cells compared to hK3 cells (Fig. 5C and Video 13). As seen in Video 13, the entire surface of hK3pxn expressing cells (red, on the top of the screen) was “bubbling” with large round blebs, whereas hK3 cells (green, bottom of the screen) primarily formed sharper lamellipodia-like structures, which were substantially smaller and restricted to ~30% of the surface area of the cell. Quantification of blebbing in Fig. 5D revealed than while 30% of hK3 cells did not form any blebs or lamellipodia, all of the hK3pxn cells showed extensive blebbing. The protrusions turned over quickly, and there was no difference in the relative lifetime between hK3 cells and hK3pxn cells in 3D (Fig. S4E). Taken together, these results show that Kindlin-3-PXN/LPXN interactions restrict macrophage migration and membrane blebbing, thereby preventing cellular transition from a slower mesenchymal to a faster amoeboid mode.

Disruption of Kindlin-3-PXN/LPXN interaction promotes macrophage phagocytosis

Phagocytosis, which is the main function of macrophages, aims to remove cell debris and microbial pathogens (43). Phagocytosis of particles covered with C3bi complement component depends on the $\alpha_M\beta 2$ integrin and its Kindlin-3 dependent activation by an agonist (8). PMA stimulation leads to 5.6 fold increase in the number of phagocytosed beads per control cell demonstrating that the process is, indeed, is entirely dependent on agonist stimulation (Fig. 6A, 6B). At the same time, heat-inactivation of C3bi complement component on the beads completely abolished phagocytosis showing the specificity of this assay (Fig. 6A, 6B). The lack of Kindlin-3 in K3KO cells abolished phagocytosis of C3bi covered beads even after PMA treatment (Fig. 6A, 6B), which is consistent with a deficient ligand recognition by K3KO cells. Re-expression of hK3 in both independent K3KO#1 and K3KO#2 CRISPR macrophage lines completely rescued their phagocytic function to an average number of 40 beads and 30 beads per cell respectively upon PMA stimulation (Fig. 6C, 6D), which is nearly identical to the number of beads per control cell prior to Kindlin-3 deletion, emphasizing the key role of Kindlin-3 in phagocytosis. The direct comparison between hK3 and hK3pxn mutant in K3KO cells revealed that PMA-stimulated hK3pxn mutant cells phagocytosed ~45% and 30% more beads per cell compared to hK3 in K3KO#1 and K3KO#2 lines, respectively (Fig. 6C, 6D). These responses were specific and were completely abolished by heat shock treatment (Fig. 6C, 6D). Increased phagocytosis of hK3pxn cells was consistent with their augmented membrane blebbing, which is known to

favor phagocytic and endocytic events (44). Together, these results show that Kindlin-3-PXN/LPXN binding restricts macrophage phagocytosis.

Discussion

Our study has identified PXN and LPXN as new and direct intracellular binding partners for a key regulator of myeloid cells, Kindlin-3, and it has defined its structure-functional significance in myeloid cell biology. NMR and pull-down approaches identified G43/L47 residues, which are conserved amongst all Kindlin paralogs, within the Kindlin-3 F0 domain as a binding site for both, PXN and LPXN. Site-directed mutagenesis, equal re-expression of mutants in two independent CRISPR macrophage lines, and a subsequent analysis of integrin-dependent functions in macrophages revealed that this Kindlin-3-PXN/LPXN interaction stands apart from interactions with other known partners for Kindlin-3, as well as from the interaction between Kindlin-2 and PXN. While other adhesome binding partners of Kindlins, including ILK and actin, were shown to promote their integrin-dependent functions (24, 45), this interaction seems to have an inhibitory role for integrin-mediated macrophage responses. Disruption of Kindlin-3 and PXN/LPXN binding augments cell spreading, increases cell polarization and formation of protrusions on the substrate, increases cell blebbing, promoting protrusions turnover and the transition from mesenchymal to faster amoeboid mode of migration, increases cell velocity and, finally, augments phagocytosis. The lack of Kindlin-3- PXN/LPXN binding does not substantially interfere with ligand recognition by integrins and, therefore, does not impact cell adhesion. Kindlin-3 binding to integrin cytoplasmic domain does not affect Kindlin-3-PXN/LPXN interaction, therefore these sites operate independently. Most importantly, disruption of this link between Kindlin-3 and the cytoskeleton destabilizes the membrane, leading to augmented blebbing and faster protrusions turnover, which, in turn, permits a high rate of migration and increases phagocytosis, which are two of the main functions of macrophages. Cell blebbing is an important prerequisite for a switch to the faster amoeboid migration, which is generally adhesion-independent and does not require functions of integrins or their activators, Talin (19, 46) and Kindlin-3 (47). It was shown previously that adhesion-free conditions or diminished integrin function or expression are sufficient to force a mesenchymal-to-amoeboid transition when cells are exposed to confinement (16). This explains the movement of adhesion-deficient Kindlin-3-null cells in 3D *in vivo* and extensive blebbing of K3KO cells in both, 2D and 3D conditions. One of the paradoxical aspects of K3pxn mutant is the combination of high adhesiveness with extensive blebbing, which is indicative of high amoeboid migration potential. High adhesiveness is expected to slow down both, spontaneous and directed cell migration (16); however, this is not the case for the K3pxn mutant.

Interestingly, while Kindlin-3-PXN binding (Kd =117.2±6.0 μM) is stronger than Kindlin-2-PXN binding (Kd=200.8±7.2 μm) (27), the Kindlin-2 F2 domain binds much stronger to the integrin-linked kinase (ILK)–PINCH–Parvin complex compared to Kindlin-3 (45). In contrast to Kindlin-3, Kindlin-2 localizes to focal adhesions where other components of “adhesome”, such as ILK are recruited (45). Thus, mechanistically, Kindlin-3 binding to PXN might compensate for the weak interaction with other cytoskeletal proteins, exemplified by ILK (45), representing the main link to the cytoskeleton. In addition, while

stable focal adhesions are characteristic for cells expressing Kindlin-2, Kindlin-3-expressing cells do not form stable contacts with extracellular matrix (ECM). Leukocytes, circulating in the blood or lymph in a cocktail of soluble ligands, such as fibrinogen and fibronectin, are programmed to avoid ECM interactions, since integrin-ligand binding results in immediate immobilization of these cells, either within the blood clot or on the surface of the inflamed endothelium (48–50). It appears that in contrast to Kindlin-2, which requires an interaction with the cytoskeleton to support integrin-dependent functions, Kindlin-3 binding to the cytoskeletal adaptor PXN serves as an inhibitory connection, restricting cell adhesiveness and preserving membrane stability to limit amoeboid cell migration and excessive phagocytosis. Thus, the consequences of Kindlin-3 anchoring to the cytoskeleton are opposite to that of Kindlin-2, demonstrating one of the first critical distinctions between Kindlin paralogs.

There are a number of discrepancies in the literature between the effects of individual Kindlin or PXN knockouts in various cells. For instance, PXN was shown to generally promote integrin-dependent functions in most Kindlin-2 expressing cells (51), however, in platelets, PXN seems to have an opposite effect (52). These studies point highlight the differences between Kindlin-2 expressing cells with their dependence on stable focal adhesions containing numerous binding partners for Kindlins and Kindlin-3 expressing hematopoietic cells lacking stable focal adhesions.

Since amoeboid migration is a feature of myeloid precursor cells, whereas a more adhesive and elongated shape is a signature of more mature macrophages (53), it seems that Kindlin-3 interactions with cytoplasmic proteins, including PXN, might be associated with myeloid cell maturation and/or neoplastic transformation. Indeed, the acquisition of the amoeboid migration serves as a key feature of cancer transformation and aggressiveness (54). We have predicted several cancer-associated mutations that might directly interfere with the Kindlin-3-PXN binding interface. Kindlin-3 L46F mutant in human Mucinous Stomach Adenocarcinoma and G44E mutant in human prostate cancer (data from 11K cases and all TCGA tumor types) (55–60) (Fig. S4F) might drive tumorigenesis by reducing Kindlin-3-PXN/LPXN binding.

Together, we show that a new regulatory pathway suppressing myeloid cell adhesion, extensive blebbing associated with amoeboid motility and phagocytosis, thereby affecting not only immune defense but also pathogenesis of inflammatory, degenerative diseases and cancer.

Supplementary Material

Refer to Web version on PubMed Central for supplementary material.

Acknowledgments:

We acknowledge the Cleveland Clinic Imaging Core and Flow Core equipment and services. We would like to thank Michael McCoy and Greg DeGirolamo for useful discussions, and Chris Nelson, Gautam Mahajan, Daniel Nascimento, and Evan Welch for manuscript proofing.

This work was supported by NIH (National Institutes of Health) grants HL071625 and HL142772 of the United States.

The abbreviation used are

K3	Kindlin-3
K3pxn	Kindlin-3-G43K/L47E mutant
K3KO	Kindlin-3 knockout
NMR	Nuclear Magnetic Resonance spectroscopy
HSQC	heteronuclear single quantum coherence

References

1. Wynn TA, Chawla A, and Pollard JW. 2013. Macrophage biology in development, homeostasis and disease. Nature 496: 445–455. [PubMed: 23619691]
2. Kim KW, Zhang N, Choi K, and Randolph GJ. 2016. Homegrown Macrophages. Immunity 45: 468–470. [PubMed: 27653599]
3. Renkawitz J, and Sixt M. 2010. Mechanisms of force generation and force transmission during interstitial leukocyte migration. EMBO Rep 11: 744–750. [PubMed: 20865016]
4. Friedl P, and Weigelin B. 2008. Interstitial leukocyte migration and immune function. Nat Immunol 9: 960–969. [PubMed: 18711433]
5. Zaidel-Bar R, Itzkovitz S, Ma'ayan A, Iyengar R, and Geiger B. 2007. Functional atlas of the integrin adhesome. Nat Cell Biol 9: 858–867. [PubMed: 17671451]
6. Horton ER, Humphries JD, James J, Jones MC, Askari JA, and Humphries MJ. 2016. The integrin adhesome network at a glance. Journal of cell science 129: 4159–4163. [PubMed: 27799358]
7. Plow EF, Meller J, and Byzova TV. 2014. Integrin function in vascular biology: a view from 2013. Curr Opin Hematol 21: 241–247. [PubMed: 24626045]
8. Malinin NL, Zhang L, Choi J, Ciocea A, Razorenova O, Ma YQ, Podrez EA, Tosi M, Lennon DP, Caplan AI, Shurin SB, Plow EF, and Byzova TV. 2009. A point mutation in KINDLIN3 ablates activation of three integrin subfamilies in humans. Nat Med 15: 313–318. [PubMed: 19234460]
9. Stadtmann A, and Zarbock A. 2017. The role of kindlin in neutrophil recruitment to inflammatory sites. Curr Opin Hematol 24: 38–45. [PubMed: 27749372]
10. Meller J, Chen Z, Dudiki T, Cull RM, Murtazina R, Bal SK, Pluskota E, Stefl S, Plow EF, Trapp BD, and Byzova TV. 2017. Integrin-Kindlin3 requirements for microglial motility in vivo are distinct from those for macrophages. JCI Insight 2.
11. Friedl P, and Wolf K. 2010. Plasticity of cell migration: a multiscale tuning model. J Cell Biol 188: 11–19. [PubMed: 19951899]
12. Petrie RJ, and Yamada KM. 2016. Multiple mechanisms of 3D migration: the origins of plasticity. Curr Opin Cell Biol 42: 7–12. [PubMed: 27082869]
13. Small JV, Stradal T, Vignal E, and Rottner K. 2002. The lamellipodium: where motility begins. Trends Cell Biol 12: 112–120. [PubMed: 11859023]
14. Chhabra ES, and Higgs HN. 2007. The many faces of actin: matching assembly factors with cellular structures. Nat Cell Biol 9: 1110–1121. [PubMed: 17909522]
15. Bergert M, Chandradoss SD, Desai RA, and Paluch E. 2012. Cell mechanics control rapid transitions between blebs and lamellipodia during migration. Proceedings of the National Academy of Sciences of the United States of America 109: 14434–14439. [PubMed: 22786929]
16. Liu YJ, Le Berre M, Lautenschlaeger F, Maiuri P, Callan-Jones A, Heuze M, Takaki T, Voituriez R, and Piel M. 2015. Confinement and low adhesion induce fast amoeboid migration of slow mesenchymal cells. Cell 160: 659–672. [PubMed: 25679760]

17. Ruprecht V, Wieser S, Callan-Jones A, Smutny M, Morita H, Sako K, Barone V, Ritsch-Marte M, Sixt M, Voituriez R, and Heisenberg CP. 2015. Cortical contractility triggers a stochastic switch to fast amoeboid cell motility. Cell 160: 673–685. [PubMed: 25679761]

18. Chikina AS, Svitkina TM, and Alexandrova AY. 2019. Time-resolved ultrastructure of the cortical actin cytoskeleton in dynamic membrane blebs. J Cell Biol 218: 445–454. [PubMed: 30541746]

19. Lammermann T, Bader BL, Monkley SJ, Worbs T, Wedlich-Soldner R, Hirsch K, Keller M, Forster R, Critchley DR, Fassler R, and Sixt M. 2008. Rapid leukocyte migration by integrin-independent flowing and squeezing. Nature 453: 51–55. [PubMed: 18451854]

20. Li H, Deng Y, Sun K, Yang H, Liu J, Wang M, Zhang Z, Lin J, Wu C, Wei Z, and Yu C. 2017. Structural basis of kindlin-mediated integrin recognition and activation. Proceedings of the National Academy of Sciences of the United States of America 114: 9349–9354. [PubMed: 28739949]

21. Liu J, Fukuda K, Xu Z, Ma YQ, Hirbawi J, Mao X, Wu C, Plow EF, and Qin J. 2011. Structural basis of phosphoinositide binding to kindlin-2 protein pleckstrin homology domain in regulating integrin activation. J Biol Chem 286: 43334–43342. [PubMed: 22030399]

22. Shi X, Ma YQ, Tu Y, Chen K, Wu S, Fukuda K, Qin J, Plow EF, and Wu C. 2007. The MIG-2/integrin interaction strengthens cell-matrix adhesion and modulates cell motility. J Biol Chem 282: 20455–20466. [PubMed: 17513299]

23. Kadry YA, Huet-Calderwood C, Simon B, and Calderwood DA. 2018. Kindlin-2 interacts with a highly conserved surface of ILK to regulate focal adhesion localization and cell spreading. Journal of cell science 131.

24. Bledzka K, Bialkowska K, Sossey-Alaoui K, Vaynberg J, Pluskota E, Qin J, and Plow EF. 2016. Kindlin-2 directly binds actin and regulates integrin outside-in signaling. J Cell Biol 213: 97–108. [PubMed: 27044892]

25. Bottcher RT, Veelders M, Rombaut P, Faix J, Theodosiou M, Stradal TE, Rottner K, Zent R, Herzog F, and Fassler R. 2017. Kindlin-2 recruits paxillin and Arp2/3 to promote membrane protrusions during initial cell spreading. J Cell Biol 216: 3785–3798. [PubMed: 28912124]

26. Theodosiou M, Widmaier M, Bottcher RT, Rognoni E, Veelders M, Bharadwaj M, Lambacher A, Austen K, Muller DJ, Zent R, and Fassler R. 2016. Kindlin-2 cooperates with talin to activate integrins and induces cell spreading by directly binding paxillin. Elife 5: e10130. [PubMed: 26821125]

27. Zhu L, Liu H, Lu F, Yang J, Byzova TV, and Qin J. 2019. Structural Basis of Paxillin Recruitment by Kindlin-2 in Regulating Cell Adhesion. Structure.

28. Liu Y, Zhu Y, Ye S, and Zhang R. 2012. Crystal structure of kindlin-2 PH domain reveals a conformational transition for its membrane anchoring and regulation of integrin activation. Protein Cell 3: 434–440. [PubMed: 22653426]

29. Gao J, Huang M, Lai J, Mao K, Sun P, Cao Z, Hu Y, Zhang Y, Schulte ML, Jin C, Wang J, White GC, Xu Z, and Ma YQ. 2017. Kindlin supports platelet integrin alphaIIbbeta3 activation by interacting with paxillin. Journal of cell science 130: 3764–3775. [PubMed: 28954813]

30. Brynn Hibbert D, and Thordarson P. 2016. The death of the Job plot, transparency, open science and online tools, uncertainty estimation methods and other developments in supramolecular chemistry data analysis. Chem Commun (Camb) 52: 12792–12805. [PubMed: 27779264]

31. Rognoni E, Ruppert R, and Fassler R. 2016. The kindlin family: functions, signaling properties and implications for human disease. Journal of cell science 129: 17–27. [PubMed: 26729028]

32. Yates LA, Fuzery AK, Bonet R, Campbell ID, and Gilbert RJ. 2012. Biophysical analysis of Kindlin-3 reveals an elongated conformation and maps integrin binding to the membrane-distal beta-subunit NPXY motif. J Biol Chem 287: 37715–37731. [PubMed: 22989875]

33. Schaller MD 2001. Paxillin: a focal adhesion-associated adaptor protein. Oncogene 20: 6459–6472. [PubMed: 11607845]

34. Brown MC, and Turner CE. 2004. Paxillin: adapting to change. Physiological reviews 84: 1315–1339. [PubMed: 15383653]

35. Tumbarello DA, Brown MC, Hetey SE, and Turner CE. 2005. Regulation of paxillin family members during epithelial-mesenchymal transformation: a putative role for paxillin delta. Journal of cell science 118: 4849–4863. [PubMed: 16219691]

36. Vaynberg J, and Qin J. 2006. Weak protein-protein interactions as probed by NMR spectroscopy. Trends Biotechnol 24: 22–27. [PubMed: 16216358]
37. Weber C, Kitayama J, and Springer TA. 1996. Differential regulation of beta 1 and beta 2 integrin avidity by chemoattractants in eosinophils. Proceedings of the National Academy of Sciences of the United States of America 93: 10939–10944. [PubMed: 8855287]
38. Diz-Munoz A, Krieg M, Bergert M, Ibarlucea-Benitez I, Muller DJ, Paluch E, and Heisenberg CP. 2010. Control of directed cell migration in vivo by membrane-to-cortex attachment. PLoS Biol 8: e1000544. [PubMed: 21151339]
39. Chenoweth DE, Cooper SW, Hugli TE, Stewart RW, Blackstone EH, and Kirklin JW. 1981. Complement activation during cardiopulmonary bypass: evidence for generation of C3a and C5a anaphylatoxins. The New England journal of medicine 304: 497–503. [PubMed: 7453783]
40. Guo RF, and Ward PA. 2005. Role of C5a in inflammatory responses. Annu Rev Immunol 23: 821–852. [PubMed: 15771587]
41. Ward PA 2004. The dark side of C5a in sepsis. Nat Rev Immunol 4: 133–142. [PubMed: 15040586]
42. Keren K. 2011. Cell motility: the integrating role of the plasma membrane. Eur Biophys J 40: 1013–1027. [PubMed: 21833780]
43. Rougerie P, Miskolci V, and Cox D. 2013. Generation of membrane structures during phagocytosis and chemotaxis of macrophages: role and regulation of the actin cytoskeleton. Immunol Rev 256: 222–239. [PubMed: 24117824]
44. Diz-Munoz A, Fletcher DA, and Weiner OD. 2013. Use the force: membrane tension as an organizer of cell shape and motility. Trends Cell Biol 23: 47–53. [PubMed: 23122885]
45. Huet-Calderwood C, Brahme NN, Kumar N, Stiegler AL, Raghavan S, Boggon TJ, and Calderwood DA. 2014. Differences in binding to the ILK complex determines kindlin isoform adhesion localization and integrin activation. Journal of cell science 127: 4308–4321. [PubMed: 25086068]
46. Lammermann T, and Sixt M. 2009. Mechanical modes of 'amoeboid' cell migration. Curr Opin Cell Biol 21: 636–644. [PubMed: 19523798]
47. Meller J, Rogozin IB, Poliakov E, Meller N, Bedanov-Pack M, Plow EF, Qin J, Podrez EA, and Byzova TV. 2015. Emergence and subsequent functional specialization of kindlins during evolution of cell adhesiveness. Mol Biol Cell 26: 786–796. [PubMed: 25540429]
48. Obenauf AC, and Massagué J. 2015. Surviving at a Distance: Organ-Specific Metastasis. Trends in Cancer 1: 76–91. [PubMed: 28741564]
49. Schwartz MA, Vestweber D, and Simons M. 2018. A unifying concept in vascular health and disease. Science (New York, N.Y.) 360: 270–271.
50. Yurdagul A Jr., and Orr AW. 2016. Blood Brothers: Hemodynamics and Cell-Matrix Interactions in Endothelial Function. Antioxidants & redox signaling 25: 415–434. [PubMed: 26715135]
51. Deakin NO, and Turner CE. 2008. Paxillin comes of age. Journal of cell science 121: 2435–2444. [PubMed: 18650496]
52. Sakata A, Ohmori T, Nishimura S, Suzuki H, Madoiwa S, Mimuro J, Kario K, and Sakata Y. 2014. Paxillin is an intrinsic negative regulator of platelet activation in mice. Thrombosis journal 12: 1. [PubMed: 24383745]
53. McNally AK, and Anderson JM. 2002. β1 and β2 Integrins Mediate Adhesion during Macrophage Fusion and Multinucleated Foreign Body Giant Cell Formation. The American Journal of Pathology 160: 621–630. [PubMed: 11839583]
54. Krakhmal NV, Zavyalova MV, Denisov EV, Vtorushin SV, and Perelmuter VM. 2015. Cancer Invasion: Patterns and Mechanisms. Acta naturae 7: 17–28. [PubMed: 26085941]
55. Ellrott K, Bailey MH, Saksena G, Covington KR, Kandoth C, Stewart C, Hess J, Ma S, Chiotti KE, McLellan M, Sofia HJ, Hutter C, Getz G, Wheeler D, Ding L, Group MCW, and N. Cancer Genome Atlas Research. 2018. Scalable Open Science Approach for Mutation Calling of Tumor Exomes Using Multiple Genomic Pipelines. Cell Syst 6: 271–281 e277. [PubMed: 29596782]
56. Gao Q, Liang WW, Foltz SM, Mutharasu G, Jayasinghe RG, Cao S, Liao WW, Reynolds SM, Wyczalkowski MA, Yao L, Yu L, Sun SQ, Fusion Analysis Working G, N. Cancer Genome Atlas Research, K. Chen AJ Lazar RC Fields MC Wendl BA Van Tine R. Vij F. Chen M. Nykter,

Shmulevich, and Ding L. 2018. Driver Fusions and Their Implications in the Development and Treatment of Human Cancers. Cell Rep 23: 227–238 e223. [PubMed: 29617662]

57. Hoadley KA, Yau C, Hinoue T, Wolf DM, Lazar AJ, Drill E, Shen R, Taylor AM, Cherniack AD, Thorsson V, Akbani R, Bowlby R, Wong CK, Wiznerowicz M, Sanchez-Vega F, Robertson AG, Schneider BG, Lawrence MS, Noushmehr H, Malta TM, N. Cancer Genome Atlas, Stuart JM, Benz CC, and Laird PW. 2018. Cell-of-Origin Patterns Dominate the Molecular Classification of 10,000 Tumors from 33 Types of Cancer. Cell 173: 291–304 e296. [PubMed: 29625048]
58. Liu J, Lichtenberg T, Hoadley KA, Poisson LM, Lazar AJ, Cherniack AD, Kovatich AJ, Benz CC, Levine DA, Lee AV, Omberg L, Wolf DM, Shriver CD, Thorsson V, N. Cancer Genome Atlas Research, and Hu H. 2018. An Integrated TCGA Pan-Cancer Clinical Data Resource to Drive High-Quality Survival Outcome Analytics. Cell 173: 400–416 e411. [PubMed: 29625055]
59. Sanchez-Vega F, Mina M, Armenia J, Chatila WK, Luna A, La KC, Dimitriadoy S, Liu DL, Kantheti HS, Saghafinia S, Chakravarty D, Daian F, Gao Q, Bailey MH, Liang WW, Foltz SM, Shmulevich I, Ding L, Heins Z, Ochoa A, Gross B, Gao J, Zhang H, Kundra R, Kandoth C, Bahceci I, Dervishi L, Dogrusoz U, Zhou W, Shen H, Laird PW, Way GP, Greene CS, Liang H, Xiao Y, Wang C, Iavarone A, Berger AH, Bivona TG, Lazar AJ, Hammer GD, Giordano T, Kwong LN, McArthur G, Huang C, Tward AD, Frederick MJ, McCormick F, Meyerson M, N. Cancer Genome Atlas Research, E. M. Van Allen AD Cherniack G. Ciriello C. Sander, and Schultz N. 2018. Oncogenic Signaling Pathways in The Cancer Genome Atlas. Cell 173: 321–337 e310. [PubMed: 29625050]
60. Taylor AM, Shih J, Ha G, Gao GF, Zhang X, Berger AC, Schumacher SE, Wang C, Hu H, Liu J, Lazar AJ, N. Cancer Genome Atlas Research, A. D. Cherniack R. Beroukhim, and Meyerson M. 2018. Genomic and Functional Approaches to Understanding Cancer Aneuploidy. Cancer Cell 33: 676–689 e673. [PubMed: 29622463]

Key points:

1. Kindlin-3-PXN/LPXN interact by F0 domain of Kindlin-3 and LIM4 domain of PXN/LPXN.
2. Kindlin-3-PXN/LPXN link limits membrane blebbing and macrophage migration.
3. Kindlin-3-PXN/LPXN interactions inhibit macrophage phagocytosis.

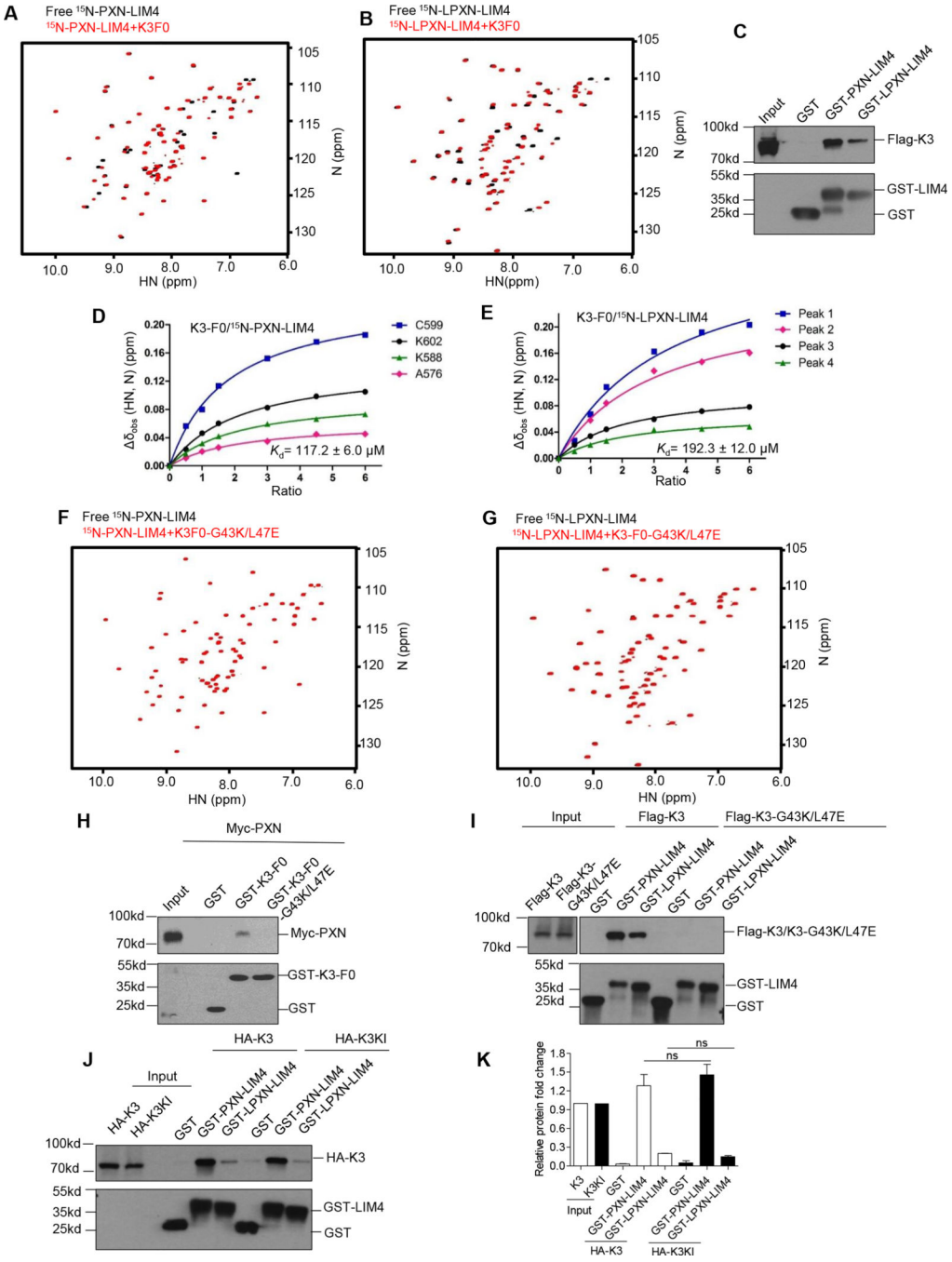

Figure 1. Kindlin-3 F0 interacts with both LIM4 domains of PXN and LPXN

(**A**) NMR 2D-HSQC shows that the PXN LIM4 domain interacts with the Kindlin-3 F0 domain. The HSQC spectra of 100 μM ^{15}N-labeled PXN-LIM4 in the absence (black) and presence of 300 μM Kindlin-3 F0 (red) are shown. (**B**) NMR 2D-HSQC shows that the LPXN LIM4 domain interacts with the Kindlin-3 F0 domain. The HSQC spectra of 100 μM ^{15}N-labeled LPXN-LIM4 in the absence (black) and presence of 300 μM Kindlin-3 F0 (red) are shown. (**C**) GST pull-down demonstrates the interaction between flag-Kindlin-3 expressed in HEK293 cells with both GST-PXN and GST-LPXN. (**D**) The affinity of

Kindlin-3 F0 binding to the PXN LIM4 domain (K_d: 117.2 μM) measured by HSQC titration. Titration curves of four representative residues are shown. (**E**) The affinity of Kindlin-3 F0 binding to the LPXN LIM4 domain (K_d: 192.3 μM) measured by HSQC titration. Titration curves of four representative resonance peaks are shown. (**F**) The HSQC spectra of 100 μM ^{15}N-labeled PXN-LIM4 in the absence (black) and presence of 300 μM Kindlin-3 F0-G43K/L47E mutant (red) suggest that G43K/L47E mutations block Kindlin-3 F0 binding to PXN-LIM4. (**G**) The HSQC spectra of 100 μM ^{15}N-labeled LPXN LIM4 domain in the absence (black) and presence of 300 μM Kindlin-3 F0-G43K/L47E mutant (red) suggest that G43K/L47E mutations block Kindlin-3 F0 binding to LPXN-LIM4. Values=mean±S.D. (**H**) GST pull-down assay demonstrates that Myc-PXN expressed in HEK293 cells interacts with GST-Kindlin-3-F0 by conserved Kindlin-3-F0-G43/L47. (**I**) GST pull-down assay demonstrates Flag-Kindlin-3, but not Flag-Kindlin-3-G43K/L47E expressed in HEK293 cells, interacts with GST-PXN-LIM4 and GST-LPXN-LIM4. (**J**) GST pull-down assay demonstrates interactions between both HA-Kindlin-3 (FL, full length) and HA-K3KI (Kindlin-3 mutant, that does not bind to integrin) with PXN/LPXN-LIM4 domain. (**K**) Quantification of Western blotting shows similar binding of HA-Kindlin-3 (FL, full length) and HA-K3KI with PXN/LPXN-LIM4, n=2.

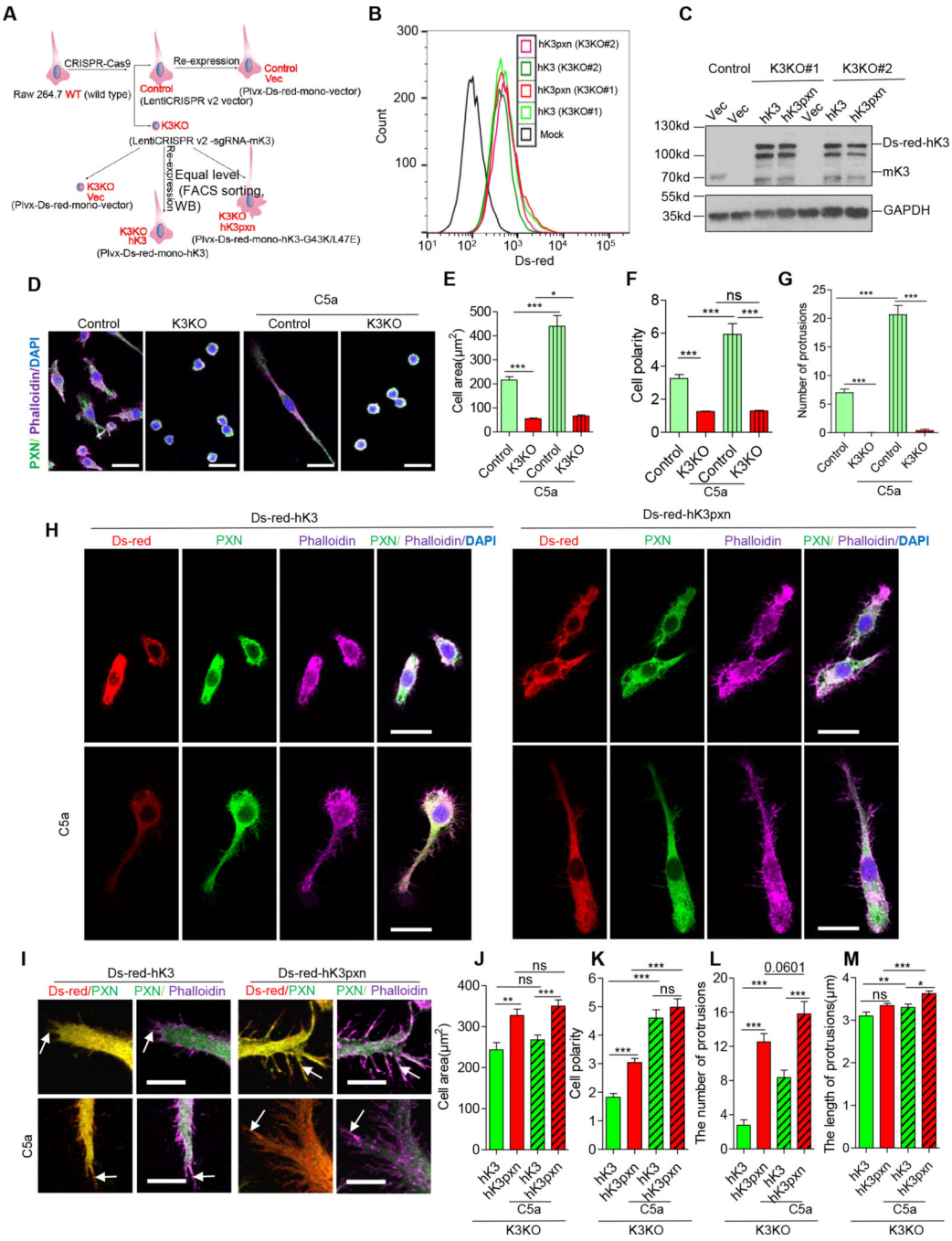

Figure 2. Disruption of Kindlin-3-PXN/LPXN interactions promote cell spreading, cell polarity, and an increase in the number of cell protrusions

(**A**) A representative schematic of generating process of K3KO and their rescued cells. K3KO cells were generated by CRISPR-cas9 and then re-expressed vector (Vec) (Plvx-ds-red-mono vector), human Kindlin-3 (hK3) (Plvx-ds-red-mono-hK3) or human Kindlin-3 (hK3pxn) (Plvx-ds-red-mono-hK3-G43K/L47E), respectively, by lentiviral infection. (**B**) Flow cytometry analysis demonstrates equal levels of hK3 and hK3pxn expression in K3KO cell lines based on the Ds-Red signal. K3KO cells with hK3 and hK3pxn were analyzed by

flow cytometry. Wild-type cells were used as Mock (negative control). (**C**) Western blot showing equal levels of hK3 and hK3pxn expression in K3KO Raw264.7 cells. The protein levels of Kindlin-3 were detected, using an antibody for mouse Kindlin3 (mK3), human Kindlin-3 (Ds-red- hK3), and GAPDH was used as a loading control. Both, mouse Kindlin-3 (mK3) and human K3 (hK3)-Ds-Red fusion are indicated. (**D**) Confocal images of Control cells and K3KO cells seeded on fibronectin pre-coated coverslips for 2 hours with or without 20ng/ml C5a treatment. Staining for PXN (green), F-actin (purple, Alexa-Fluor 647-Phalloidin) and DAPI are shown. Scale bar=20μm. (**E, F**) Quantification of cell area and cell polarity in Control and K3KO cells. Control (without C5a, n=35, and with C5a, n=34) and K3KO (without C5a, n=34, and with C5a n=27).Values=means+SEM. p*<0.05, p***<0.001 based on Student's t-test. (**G**) Quantification of protrusions from Figure 2D. Control (without C5a, n=35, with C5a, n=25) and K3KO (without C5a, n=35 and with C5a, n=36).Values=means+SEM. p***<0.001 based on Student's t-test. (**H**) Confocal images of K3KO cells expressing WT Kindlin-3 (hK3) or Kindlin-3-PXN /LPXN mutant (hK3pxn) seeded on fibronectin pre-coated coverslips for 2 hours. Staining for PXN (green), F-actin (purple, Alexa-Fluor 647-Phalloidin) and DAPI are shown. Ds-red indicates the presence of hK3 or hK3pxn. Scale bar, 20μm. (**I**) Confocal images showing actin-rich protrusions of hK3 or hK3pxn cells seeded on fibronectin for 2 hours with or without 20ng/ml C5a. Staining for PXN (green), F-actin (purple, Alexa-Fluor 647-Phalloidin) and DAPI are shown. White arrows indicate cell protrusions. Scale bar=10μm. (**J**) Quantification of cell area in K3KO cells expressing either WT Kindlin-3 (hK3) or Kindlin-3-PXN/LPXN mutant (hK3pxn). K3KO with hK3 (without C5a, n=55 and with C5a, n=88) and re- hK3pxn mutant (without C5a, n=78, and with C5a, n=113).Values=means+SEM. p**<0.005 and p***<0.001 based on Student's t-test. (**K**) Quantification of cell area in K3KO cells expressing either WT Kindlin-3 (hK3) or Kindlin-3-PXN/LPXN mutant (hK3pxn). K3KO with hK3 (without C5a, n=69 and with C5a, n=85) and with hK3pxn (without C5a, n=86, and with C5a, n=96).Values=means+SEM. p***<0.001 based on Student's t-test. (**L**) Quantification of the number of protrusions from Figure 2I. K3KO with hK3 (without C5a, n=38, with C5a, n=35) and with hK3pxn (without C5a, n=38 and with C5a, n=35).Values=means+SEM. p**<0.005 and p***<0.001 based on Student's t-test. (**M**) Quantification of the number of protrusions from Figure 2I. K3KO with hK3 (without C5a, n=132, with C5a, n=354) and with hK3pxn (without C5a, n=509 and with C5a, n=648).Values=means+SEM. p*<0. 05, p**<0.005 and p***<0.001 based on Student's t-test.

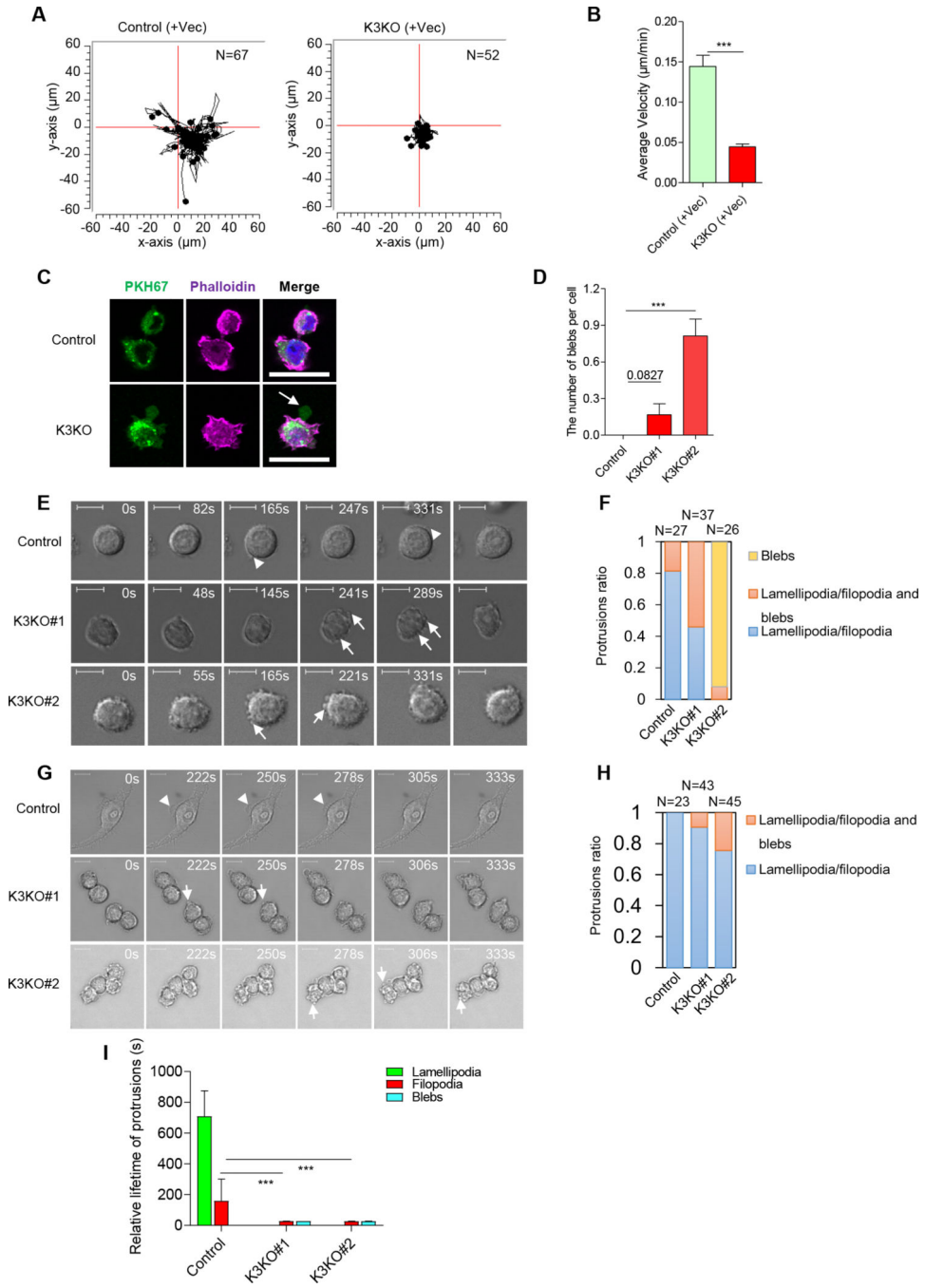

Figure 3. Knockout of Kindlin-3 augments cell velocity and promotes the transition from mesenchymal migration to amoeboid migration

(**A**) Representative tracks of CRISPR-cas9 Control cells (+Vector) and K3KO cells (+Vector) were recorded for 24 hours by phase-contrast microscopy time-lapse imaging. The starting point is at the origin, and each point represents the position of a 25min-interval. Control with Vec (n=67) and K3KO with Vec (n=52). (**B**) Quantification of the average velocity of motile cells from Figure 3A. Values=means+SEM, $p^{***}<0.001$ based on Student's *t*-test. (**C**) Representative confocal images of Control cells and K3KO cells seeded

on fibronectin for 20 min. Membrane was labeled with PKH67 (green), and Alexa-Fluor 647-Phalloidin (purple) indicates F-actin. White arrows indicate cell blebs. Scale bar, 20μm. (**D**) Quantification of blebs numbers per cell. Control (n=18), K3KO#1 (n=18), and K3KO#2 (n=32). Values=means+SEM. $p^{***}<0.001$ based on Student's *t*-test. (**E**) DIC (Differential interference contrast) microscopy time-lapse imaging showing the dynamics of cell blebbing in Control and K3KO Raw 264.7 cells at the initial adhesion stage (0–30min after plating) in 2D culture. Images of the focal layer were extracted from z-stack. White arrows and arrowheads indicate cell blebs and filopodia, respectively. Scale bar=10μm. (**F**) Ratios of various types of cell protrusions from Figure 3E in three independent experiments. Control (n=27), K3KO#1(n=37), and K3KO#2(n=26). (**G**) Bright field time-lapse imaging of cell blebbing of Control and K3KO cells at 16–18hrs after plating. Images were extracted from z-stacks. White arrows and arrowheads indicate cell blebs and lamellipodia/filopodia, respectively. Scale bar=10μm. (**H**) The ratio of cell protrusions from Figure 3G in three independent experiments. Control (n=23), K3KO#1(n=43), and K3KO#2(n=45). (I) Quantification of the relative lifetime of protrusions of Control and K3KO cells at the firm (late) adhesion stage in 2D. The average interval of each video is 27-second. Control (Lamellipodia, n=21, filopodia, n=38, and blebs, n=0), K3KO#1 (Lamellipodia, n=0, filopodia, n=121, and blebs, n=33), and K3KO#2 (Lamellipodia, n=0, filopodia, n=69, and blebs, n=68). Values=means+SEM. $p^{***}<0.001$ based on Student's *t*-test.

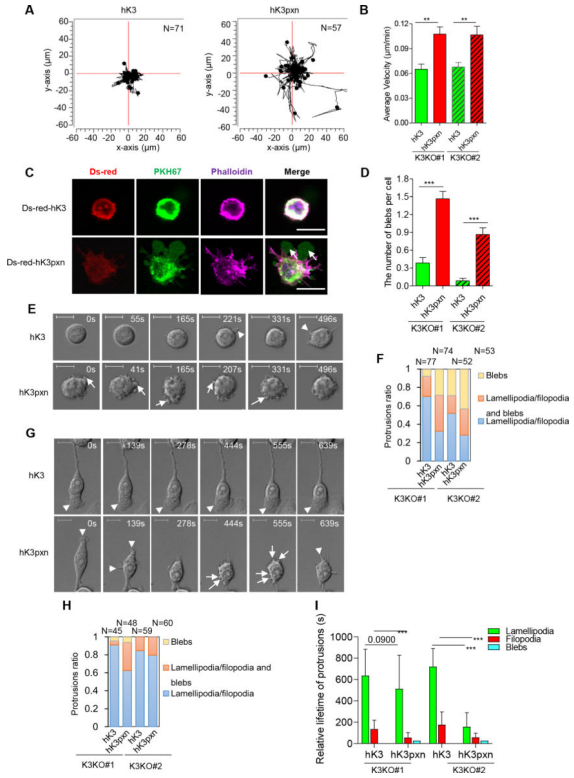

Figure 4. Disruption of Kindlin-3-PXN/LPXN interactions augments random cell velocity and promotes the transition from mesenchymal migration to amoeboid migration

(**A**) Representative tracks of K3KO Raw 264.7 cells re-expressing Kindlin-3 WT (hK3) or Kindlin-3-PXN (hK3pxn) mutant within 24 hours by phase-contrast microscopy time-lapse imaging. The starting point is at the origin, and each point represents the cell position at 25 min intervals. K3KO#1 re-expressed hK3 (n=31) and hK3pxn (n=64), and K3KO#2 re-expressed hK3 (n=71) and hK3pxn (n=57). (**B**) Bar graphs show the average velocity of cells from Figure 4A. 2.5×SD (standard deviation) was removed from consideration. Values=means+SEM, p*<0.05, p**<0.005 based on Student's t-test. (**C**) Representative confocal images of K3KO with hK3 and hK3pxn seeded on fibronectin for 20 min. Membrane was labeled with PKH67 (green), Alexa-Fluor 647-Phalloidin (purple) indicates F-actin, and Ds-red indicates hK3 and hK3pxn expression. White arrows indicate cell blebs. Scale bar, 10μm. (**D**) Quantification of blebs numbers per cell. K3KO#1 with hK3 (n=75) and hK3pxn (n=75), and K3KO#2 with hK3 (n=46) and hK3pxn (n=45) were analyzed. Values=means+SEM. p***<0.001 based on Student's t-test. (**E**) DIC microscopy time-lapse imaging showing the dynamics of cell blebbing in K3KO cells with hK3 or hK3pxn expression at the initial adhesion stage (0–30min) in 2D in three independent experiments. The images were exacted from z-stacks. White arrows and arrowheads indicate cell blebs and filopodia, respectively. Scale bar=10μm. (**F**) Characterization of cell protrusions and blebbing during adhesion. Bars show the ratios of various protrusions from Figure 4E in three independent experiments. K3KO#1 with hK3 (n=77) and hK3pxn (n=74), and K3KO#2 with hK3 (n=52) and hK3pxn (n=53) were analyzed. (**G**) DIC microscopy time-lapse imaging showing the dynamics of cell blebbing in K3KO cells with hK3 or hK3pxn expression at the firm adhesion stage (16–18hrs after seeding). Images were etrxacted from

z-stacks. White arrows and arrowheads indicate cell blebs and lamellipodia, respectively. (**H**) Characterization of cell protrusions and blebbing from Figure 4G in three independent experiments. Ratios of various protrusions types are shown. K3KO#1 with hK3 (n=45) and hK3pxn (n=48), and K3KO#2 with hK3 (n=59) and hK3pxn (n=60) were analyzed. (I) Quantification of the relative lifetime of protrusions of hK3 and hK3pxn cells at the firm adhesion stage in Figure 4G. The average interval of each video is 27-second. hK3 (K3KO#1) (Lamellipodia, n=37, filopodia, n=81, and blebs, n=0), and hK3pxn (K3KO#1) (Lamellipodia, n=25, filopodia, n=125, and blebs, n=52). hK3 (K3KO#2) (Lamellipodia, n=0, filopodia, n=17, and blebs, n=78), and hK3pxn (K3KO#2) (Lamellipodia, n=17, filopodia, n=145, and blebs, n=34). Values=means+SEM. Values=means+SEM. $p^{***}<0.001$ based on Student's t-test.

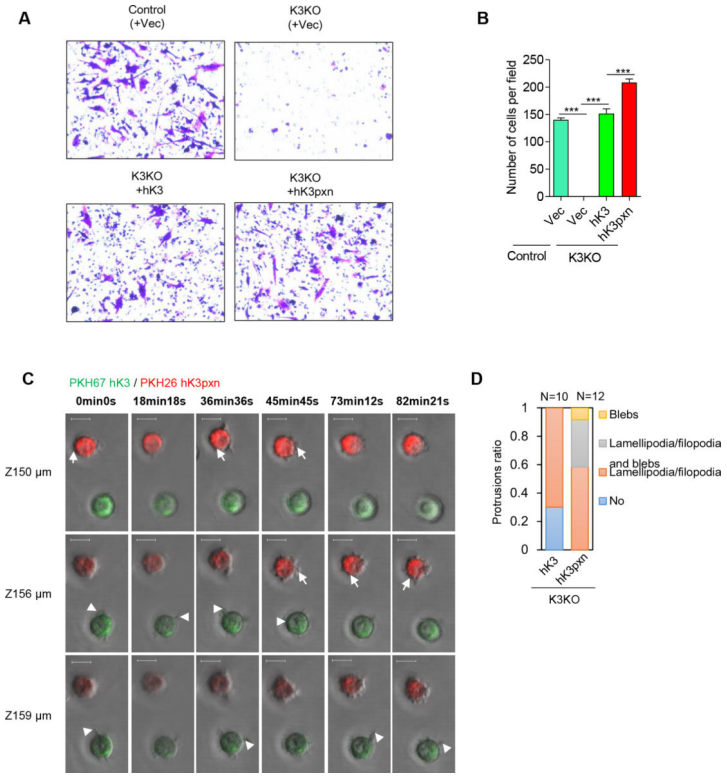

Figure 5. Disruption of Kindlin-PXN/LPXN interactions augments directed cell migration in 2D and promotes the transition from mesenchymal migration to amoeboid migration in 3D

(**A**) The K3KO cells re-expressed Kindlin-3-PXN/LPXN mutant cells (hK3pxn) migrated better than WT Kindlin-3 (hK3) in a transwell migration assay. Fibronectin was used as a ligand. (**B**) Graph shows the number of migration cells per field in three independent-experiments, with triplicates in each experiment. Control (n=15), K3KO (n=15), hK3 (n=15), and hK3pxn (n=15). Values=means+SEM, $p^{***}<0.001$ based on Student's *t*-test. (**C**) Time-lapse imaging by confocal microscopy of K3KO cells with hK3 or hK3pxn expression in the 3D fibrin gel (0–1.5hrs). Cells expressing hK3 were labeled with PKH67 membrane dye (green) and hK3pxn mutant were labeled with PKH26 membrane dye (red) and mixed together at 1:1 in 2mg/ml 3D fibrin gels at 37 ºC for 30min. After polymerization, cells in the gel (120–150 μm above the bottom) were imaged by confocal microscopy. Images were extracted from z-stacks. White arrows and arrowheads indicate cell blebs and filopodia, respectively. Scale bar=10μm. (**D**) Bars show quantification of cell protrusions from Figure 5C in three independent experiments. K3KO cells with hK3 (n=10) and hK3pxn (n=12) were analyzed.

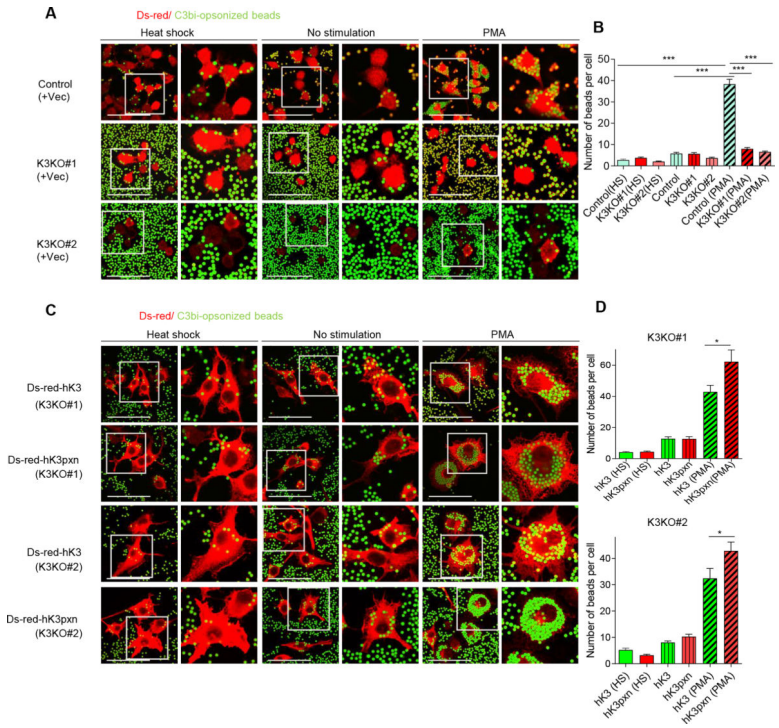

Figure 6. Kindlin-3-PXN/LPXN interactions control macrophage phagocytosis

(A) Confocal images of Control and K3KO cells phagocytosis of C3bi-opsonized Latex beads. Latex beads (carboxylate-modified polystyrene, fluorescent yellow-green) were incubated with Human IgM and fresh mouse serum with or without heat shock (HS) at 37 ºC for 1 hour to initiate C3bi-opsonization. Cells were incubated with C3bi-opsonized Latex beads with or without 150nM PMA at 37 ºC for 2 hours, then fixed, permeabilized, stained with anti-RFP antibody, and imaged by confocal microscopy. Heat shock inactivated was used as a negative control. (**B**) Bars show numbers of beads per cells in Figure 6A in the phagocytosis assay. Control (HS: n=64, no treatment: n=107, and PMA treatment: n=95), K3KO#1 (HS: n=82, no treatment: n=67, and PMA treatment: n=160), K3KO#2 (HS: n=83, no treatment: n= 46, and PMA treatment: n=131). Values=means+SEM, $p^{***}<0.001$ based on Student's *t*-test. (**C**) Representative confocal images showing phagocytosis of C3bi-opsonized Latex beads in of K3KO with hK3-or hK3pxn- expressing cells. Latex beads (carboxylate-modified polystyrene, fluorescent yellow-green) were incubated with Human IgM and fresh mouse serum with or without heat shock (HS) as indicated at 37 ºC for 1 hour to initiate C3bi-opsonization. Cells were stimulated with 150nM PMA at 37 ºC for 2 hours to activate integrins or unstimulated cells were incubated with C3bi-opsonized beads. Fixed cells were stained with anti-RFP antibody (red) to visualize hK3. Images were extracted from z-stacks by confocal microscopy. Heat shock (HS) inactive was used as a negative control. (**D**) Bars show numbers of beads per cell from Figure 6C. K3KO#1 line with hK3 (HS: n=40, no treatment: n=47, and PMA treatment: n=45), hK3pxn (HS: n=53, no treatment: n=48 and PMA treatment: n=28), K3KO#2 line with hK3 (HS: n=58, no treatment: n= 133, and PMA treatment: n=30) and hK3pxn (HS: n=89, no treatment: n=97 and PMA treatment: n=57). Values=means+SEM, $p^{*}<0.05$ based on Student's *t*-test.